Michelson Interferometer: Determining Calibration Curve and Refractive Index of Gas

[redacted]
PHY293

November 5, 2023

1 Abstract

This experiment aims to produce a calibration curve for the Michelson Interferometer and determine the refractive index of air using the Michelson Interferometer. The calibration curve demonstrates the linear relationship between the distance from the Mirror and the number of fringes observed to disappear. The refractive index of gas for air is calculated from experimental results and compared to the accepted value of 1.000277. Uncertainties are discussed and interpreted.

2 Introduction

Devices that work on the principle of the interference of superimposed waves are called interferometers. The Michelson Interferometer, is used to measure wavelengths of unknown light sources, perform sub-micrometer measurements, and investigate optical media properties.

A diagram of the Michelson Interferometer (MI), is shown in figure 1. Light from the source is divided into two beams, one that is reflected by the the glass screen G_1 , whereas the other, gets transmitted through G_1 and G_2. Both the reflected and transmitted beams get reflected back by mirrors A_1 and A_2 , respectively. The mirrors are both orthogonal to the incoming beams, which are orthogonal to the beams, and each other, causing them to interfere and create patterns, which are seen at the view-port. The viewed patterns are determined by the path difference between A_1 and A_2. Mirror A_1 can be adjusted to either increase or decrease its distance from the viewer.

There are two requirements that should be satisfied in order for fringes to appear:

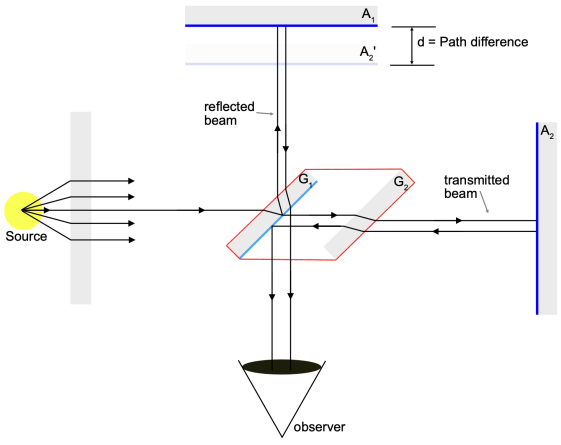

Figure 1: Michelson Interferometer Schematic (taken from the lab guide)

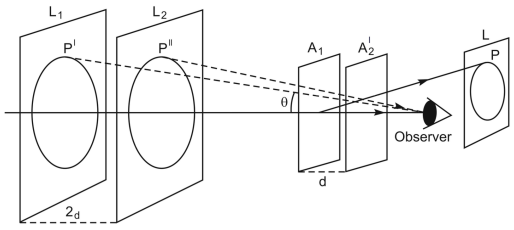

Figure 2: Visualization of the images of mirrors A_1 and A_2 (taken from the lab guide)

1. Use an extended light source to increase the area at which interference fringes appear. The fringes would be difficult to see if a discrete point source, like a laser, was used. A diffusion screen placed in front of the source (figure 1), will enlarge the surface area of the fringes.

2. Use a monochromatic light source as the spacing between beams of light is proportional to the wavelength of that light. Thus, it is more difficult to find regions of constructive interference for a larger number of distinct λ.

In order to satisfy these concerns, we use a monochromatic sodium light with a diffusion screen.

2.1 Circular Fringes and the Calibration Curve

We can assume that the extended light source L acts behind the observer, thus, the two mirrors A_1 and A_2 from figure 1 create two images L_1 and L_2 of the source L. Note that Figure 2 only holds given that A_1 and A_2 are orthogonal , otherwise, the virtual mirror of A_2, called A_2' in Figure 2 would not be parallel to the mirror A_1, resulting in non-circular fringes. depending on the tilt of mirror A_2 in Figure 1. The distance d between A_1 and A_2' varies with the use of a micrometer, the distance d translates to a distance of $2d$ by the mirrors. Thus, our first relation is when d is an integer number of half wavelengths $n\lambda_{source}/2$, then we have constructive interference, because the path difference between the images P' and P'' will have a path difference of $2 \times n\lambda_{source}/2 = n\lambda$ producing constructive interference.

$$2d\cos\theta = n\lambda \tag{1}$$

Where d is the distance between mirror A_1 and the image of mirror A_2, θ is the angle of elevation from the observer's eye to the top of image P', n is a positive integer called the fringe order and λ is the wavelength of the source.

Given that the path difference is equal to $2d\cos\theta$, we can find the phase shift by taking the ratio of the path difference relative to a full wavelength, and then multiplying by π

$$\delta = 2\pi\frac{2d\cos\theta}{\lambda} \tag{2}$$

When $\theta = 0$, we have the region of zero path difference, which leads to:

$$2dcos(0) = n\lambda \rightarrow 2d = n\lambda \tag{3}$$

Which implies that a decrease in distance of $2d$ causes a change in the order of fringe, meaning that one interference ring vanishes from sight. Thus, by rotating the micrometer, we change the fringe order, which gives the illusion of fringes appearing and disappearing. A calibration curve can be produced by measuring the number of fringes that have vanished as a function of the rotation of the micrometer.

2.2 Refractive Index of gas

The Michelson Interferometer is able to measure the refractive index of a gas by analyzing the relation of the index of refraction n and the pressure P of the gas chamber. The change in optical path length is $sl(n-1)$, thus we receive the following relationship:

$$2l(n-1) = N\lambda \tag{4}$$

Where l is the length of the gas chamber, n is the index of refraction of the gas, and N the number of fringes that have been counted. By taking the derivative of both sides w.r.t pressure, and by applying the Ideal Gas Law, the following relation is obtained:

$$n_0 = 1 + \frac{dN}{dP}\frac{\lambda}{2l}\frac{760T}{273} \tag{5}$$

Thus, by varying the pressure of the gas cell, and noting the number of disappeared fringes N at the ambient temperature $T = 298K$, we are able to find a relation for the refractive index of a gas.

3 Experimental Procedure

This section describes the equipment and apparatus used to conduct the expriment and the methods used to collect data.

3.1 Equipment and Apparatus Description

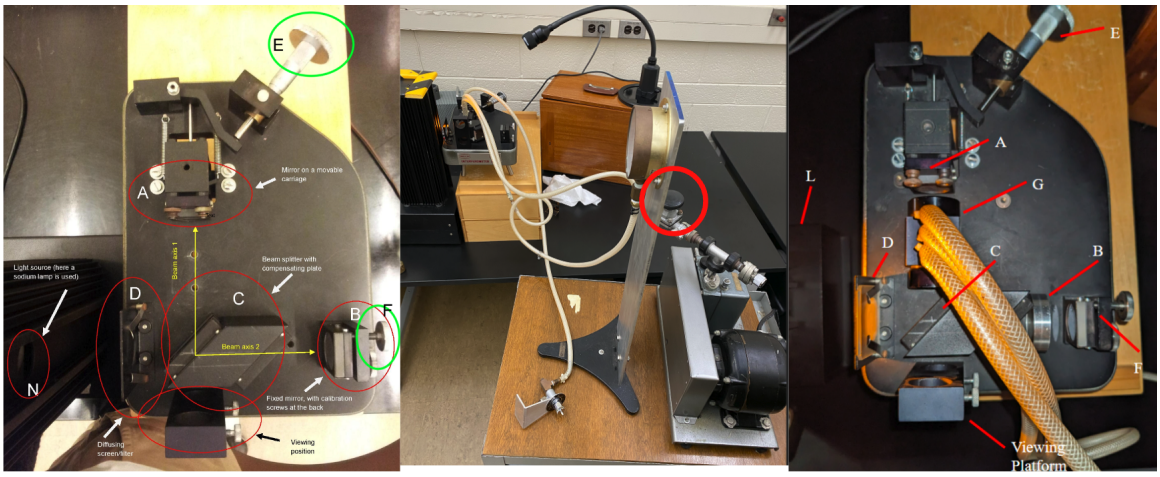

Figure 3: (a) Michelson Interferometer Components labelled for procedure 3.1. (b and c) Vacuum pump attached to the Michelson Interferometer for procedure 3.2. Source Lab Manual UofT[1]

- **Sodium lamp: (L)** Monochromatic light source with a mean sodium spectral wavelength of $\lambda = 589.3nm$
- **White Light lamp: (L)** White light source
- **Diffusing screen: (D)** A thin acrylic plate that scatters light. Increases the illuminated area where fringes can be observed.
- **Micrometer** ± 0.005 **(E):** Used to move mirror A closer or farther away from the observer, effectively manipulating the path difference between mirror A and mirror B (figure 3).

- **Vacuum pump/pressure gauge ± 20mmHg (circled in red) :** Creates a partial vacuum in the gas cell by removing air. Corresponding pressure measurements are read off the attached pressure gauge.
- **Air cell length $= 3.38 \pm 0.05$cm (G):** Reflected light from the Michelson interferometer passes through a region of pressurized gas in the air cell.
- **Compensating circular glass plates (C):** Compensates for the path difference produced by the glass walls of the gas cell, so that only the path difference produced by the gas is accounted for.

The Michelson Interferometer consists of 2 mirrors, A and B, the compensating plate C, a diffusing screen D, a micrometer E which varies the position of A, and a screw F to adjust the tilt of mirror B. The light source N is either a sodium lamp ($\lambda = 589.3nm$) or a white light source. In either case, the light source MUST pass through the diffusing screen D, according to point 1 of the introduction. The air cell, G, is connected by three reinforced plastic tubes to the vacuum pump, figure 3(b).

3.2 Procedure for Calibration Curve

The following section outlines steps taken to obtain experimental data for the calibration curve of the Michelson interferometer

3.2.1 Finding the Region of Zero Path Difference

Turn on the sodium lamp N, placing the diffusing screen in its insert D. Wait for the sodium light to emit an orange hue (5 minutes), and then turn off the lights. Start observing the image through the viewing position. Tilt mirror B, using screw F, such that the image of mirror B, aligns with that of mirror A, as in figure 1 and 2. Once both mirrors are aligned, gradually move mirror A, by rotating the micrometer E until an interference pattern is seen like in figure 4.a, which are localized parallel fringes. It will take some adjusting in order to find these parallel fringes. Once, these parallel fringes are found with the sodium light, switch over to the white light source [1]. By varying the micrometer slightly, try to find the location of zero path difference, which will appear as coloured parallel lines. You should see a pattern like in figure 4.b and 4.c, when there is interference with white light, it is known that the current micrometer reading associated to the location of zero path difference.

Figure 4: (a) Localized Parallel Fringes with monochromatic light. (b) White light, localized parallel fringes. (c) White light, localized parallel fringes. Source: Montana University [3]. Both white light patterns (b) and (c) are difficult to locate once again due to point 1 in the introduction.

[1] We first find localized fringes using the monochromatic sodium light, as the fringes are most visible. Next, we switch over to the white light, to find the region of zero path difference, because the pattern made by white light is extremely notable, but difficult to find for reasons explained in point 1 in the introduction

3.2.2 Counting the Number of Fringes

Calibration screws on mirror M2 were readjusted until large circular fringes were observed. The location of zero path difference was then found using a white light source. The micrometer position in this region was noted before switching to the the sodium light. From this location, the micrometer was rotated clockwise and the number of disappeared fringes was counted from the viewing position [2]. Every 50 fringes, the new micrometer position was noted. This was repeated 20 times, until $20 * 50 = 1000$ fringes were counted

3.3 Procedure for Refractive Index

The air cell length was measured, and then placed on the stand between mirror A and the beam splitter C. Two circular compensating plates were then placed between mirror B and the beam splitter. With the vacuum pump plugged in, the knob was rotated to increase or decrease the pressure (circled in red in figure 6.a). The vacuum pressure was initially set to 500 mm Hg. The interferometer was then adjusted until circular fringes were observable. The pressure was decreased in decrements of 100 mm Hg and the number of disappeared fringes was counted at each interval until the gauge pressure read 0 mm Hg. After the first trial, the pressure was reset to 500 mm Hg and the counting process was repeated once more.

4 Error Propagation

The following formula was used for all error propagation of calculated values:

$$\Delta f = \sqrt{\left(\frac{\partial f}{\partial x_1}\Delta x_1\right)^2 + \left(\frac{\partial f}{\partial x_2}\Delta x_2\right)^2 + \left(\frac{\partial f}{\partial x_3}\Delta x_3\right)^2 + ... + \left(\frac{\partial f}{\partial x_n}\Delta x_n\right)^2} \tag{6}$$

Where x_n is a measured value with associated uncertainty Δx_n and n is the number of different variables in the equation, f. A sample calculation is shown below for the error of displacement, Δd, in section 5.1:

$$\Delta d = \sqrt{(\frac{\partial d}{\partial n}\Delta 5)^2} = \sqrt{((\frac{\partial}{\partial n}\frac{n\lambda}{2}\Delta 5)^2} = 1473\ nm$$

5 Results

This section presents experimental data and associated uncertainties.

5.1 Calibration Curve Results

The data data collected for the calibration curve (3.1.2) and equation 3 can be used to find a relationship between the path difference, d, and micrometer movement:

$$2d = n\lambda \rightarrow d = \frac{50 \times 589.3\ nm}{2} \rightarrow d = 14733nm$$

where λ is the mean sodium spectral length. Thus, each time 50 fringes disappear from the screen, the path difference changes by 14733 nm . With this information, the change in micrometer position can be related to an actual change in displacement.

[2] Note from the perspective of the viewer, the micrometer will be turning counter clockwise

5.2 Actual Displacement

Although data collection for the number of fringes is counting from 0-1000, the fringes observed were small in dimension as seen in figures 4.a and 4.b. Thus, every 50 fringes, we account for the possibility of human error with a constant uncertainty of $\Delta n \pm 5$ fringes. The error of actual displacement, Δd, was calculated using equation (6) to be $\pm 1473nm$. Sample results are shown in table 1. Full results can be found in Appendix, figure 4. The

Fringes Disappeared (± 5)	Micrometer Reading (± 0.005)	Actual Displacement (nm) (± 1473)
0	21.27	309383
50	21.14	294650
100	21.04	279918
...	...	...
900	19.45	44198
950	19.35	29465
1000	19.24	14733

Table 1: Sample entries for the calibration curve. Micrometer reading and the actual displacement have constant uncertainties

slope of the line in figure 5 serves as our calibration, providing a conversion factor to convert micrometer units to actual displacement that occurs at the nano-scale. The *Numpy Polyfit* function was used to calculate a slope value of 148945 ± 1530, and an intercept value of -2856279 ± 31027 with uncertainties that were calculated from the covariance matrix. Thus, the conversion factor we obtain is $148945 \pm 1530 \frac{\text{nm}}{\text{micrometer reading}}$.

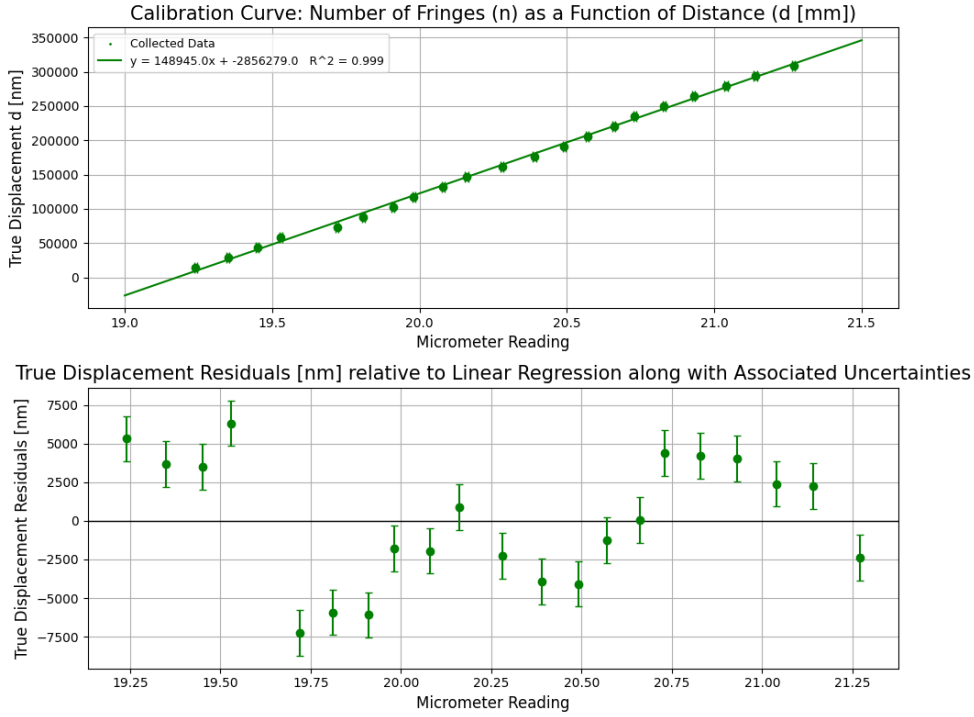

Figure 5: Calibration curve with linear regression applied as with the plotted residuals. Note that the uncertainties in the x direction are present, but are too small to be seen at the given scale.

5.3 Refractive Index of Gas Results

The number of disappeared fringes was averaged over two trials measured at the same pressure intervals as shown in table 2. The average number of fringes was not rounded to the nearest fringe because fringe count is an exact value with infinite significant figures. The slope of the figure 6 would also be less accurate if the average values were rounded.

Pressure (±20 mmHg)	Trial 1 # Fringes ±1	Trial 2 # Fringes ±1	Mean # of Fringes ±1
0	0	0	0
100	4	6	5
200	7	6	11.5
300	5	7	17.5
400	4	4	21.5
500	6	6	27.5

Table 2: Number of fringes at given values of pressure

Average number of fringes was plotted as a function of gauge pressure as shown in figure 6. The resulting fit corresponds to a linear function between the number of fringes appearing and the given gauge pressure. The Numpy Polyfit function outputs a slope value of $0.0551 \pm 0.0016 \frac{\text{number of fringes}}{\text{mmHg}}$. A plot of residuals for the graph is also shown in figure 6.

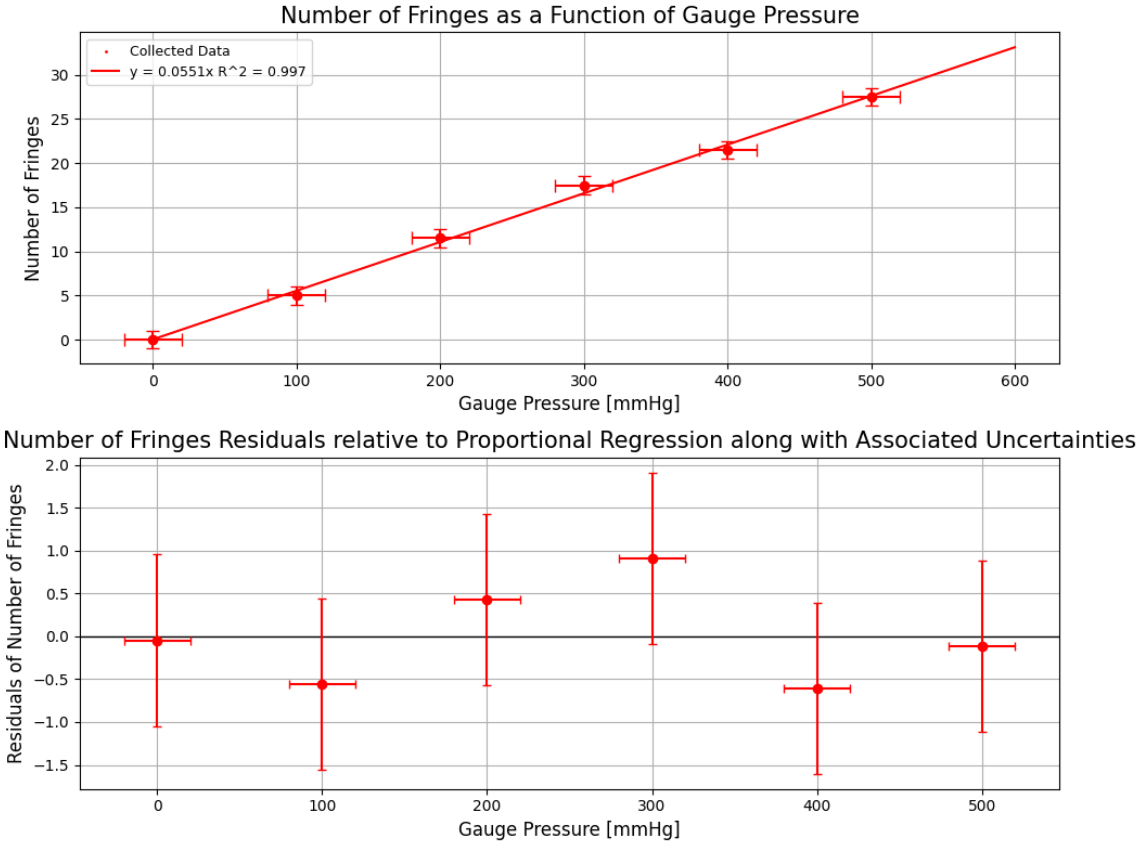

Figure 6: Fringes disappeared as a function of the gauge pressure in the gas cell.

6 Data Analysis

This section interprets experimental results.

6.1 Calibration Curve

Chi Squared Goodness of Fit Using equation (40) found in the "Error Analysis in Experimental Physical Science"[4], we calculate the value of χ^2 :

$$\chi^2 = \sum_{i=1}^{N} \frac{(y_i - f(x_i))^2}{\sigma_y^2} \rightarrow \chi^2 = \sum_{i=1}^{21} \frac{(y_i - (mx_i + b))^2}{\sigma_y^2} \tag{7}$$

Where y_i - $f(x_i)$ is the difference between the experimental value and the expected value of displacement at a specific micrometer reading and σ_y^2 is the standard deviation. In this case, by taking the values of y_i, x_i and m and b from Section 5.2 and table 1, we obtain a χ^2 value equal to 20.00. In order to find the reduced χ_ν^2, divide χ^2 by the degrees of freedom of the data set. Given that a linear fit has 2 fit parameters (m and b), and there are 21 data points, then the degree of freedom is #of fit parameters − data points or 21 - 2 = 19. Thus, $\chi_\nu^2 = \frac{20.00}{19} = 1.053$. A reduced chi squared value close to 1 indicates that our data has a good linear fit. Figure 5 visually demonstrates this, and we conclude that the screw thread was in fact uniform. This may not have been the case had we rotated the screw in both directions. Rotating clockwise and then counterclockwise by the same reading on the micrometer does not correspond to the same distance swept by the carriage. A χ_ν^2 value greater than 1 means the magnitude of experimental uncertainties were underestimated; this can be seen in the residuals plot of figure 5, where only 3 data points with their corresponding uncertainties fall within the fit.

6.2 Refractive Gas index

Using equation 5, the experimental refractive index of air was calculated. The value of $\frac{dN}{dP}$ was taken as the slope of figure 6 and three calculations were made at varying normal room temperatures, T, to account for fluctuations in temperature change during the data collection process as shown in table 3.

Temperature (K)	n_0	Uncertainty of n_0
293	1.00038	0.00005
298	1.00039	0.00001
303	1.00039	0.00006

Table 3: Index of refraction at different absolute temperatures

Uncertainties in table 3 were calculated with equation (6). The average index of refraction for air was calculated as 1.00039 ± 0.00012. The relative difference of the accepted and calculated values is shown below:

$$\frac{1.000277}{1.00039} = 0.00011 = 0.011\%$$

The calculated value also falls within one degree of uncertainty of the accepted value to the second significant figure. While this result is agreeable, it is not entirely accurate. There are different possible sources of error that are not accounted for in equation 5 which could have been overshadowed by the increased uncertainty when averaging multiple calculated values at different theoretical temperatures. For example, none of the individual temperature values in table 3 fall within one degree of uncertainty of the accepted value.

7 Error Analysis

This section discusses possible sources of error and ways to account for them.

7.1 Instrument Errors

The smallest denomination of the micrometer reading was 0.01, so its associated instrumental uncertainty is taken at a constant value of ± 0.005. Air cell measurements were done using a standard millimeter ruler so an associated uncertainty of ± 0.0005 m was used. The reading error of the pressure readout was taken as ± 20 mm Hg, half the smallest precision of the pressure gauge. Reading the pressure gauge was the largest source instrumental error because the constant change in pressure made it difficult to get a precise pressure reading. One way to account for this is to use equipment with digital readouts to avoid needle fluctuations and improve read-out precision.

7.2 Counting the Fringes

The micrometer can be moved without a complete fringe disappearing from the field of view. Similarly, the screw may rotate without the micrometer moving due to backlash between the screw thread and the mirror carriage. Backlash also becomes more severe with prolonged use of the carriage apparatus. Thus, a ± 1 fringe count was assumed to mitigate errors of this nature for data collection for the refractive index of gas. For the calibration curve, the fringes disappeared very quickly, so it was very easy to miss or double count fringes especially over a prolonged period of counting. Therefore, as additional ± 4 fringes was added to the ± 1 fringe count for an assumed ± 5 fringe uncertainty to mitigate manual counting errors for the calibration curve. To mitigate this source of error, a camera setup could be used to record fringes. This would reduce eye fatigue experienced from prolong viewing of the reflected image to mitigate human counting error.

7.3 Change in Gas Cell Length

The length of the air cell may change when pressure is released due to the atmospheric pressure forces pushing in on the cell. Equation (4) demonstrates that optical path length is linearly proportionate to cell length. When path length is changed, the calculated refractive index of a gas will also change.

7.4 Influence of Relative Humidity of Air

Moist air has a lower refractivity than dry air because the refractivity of water vapor is smaller than that of air [2]. During the process of pressurizing the air cell, the partial pressures of air and vapor may not have remained constant over the data collection period. Thus, relative humidity may not be constant throughout the experiment, causing a change in refractive index that would impact the optical path length. Equation (5) assumes a constant temperature for the calculated index of refraction of gas, and because it is derived from Equation (4) it also does not account for the path length change due to a changing index of refraction. While this source of error is applicable for both the calibration curve measurements and the refractive index of air, it is highly likely to be negligible for the calibration curve measurements and conversion factor calculations because the air is not being supplied with external energy, such as pressure force. If there were errors, they would be systematic due to equation (3) not accounting for refractivity.

8 Conclusion

The Michelson Interferometer experiment provided the ability to establish a relationship between the micrometer reading and the actual displacement which was quantified as $148945 \pm 1530 \frac{nm}{micrometer\ reading}$ through linear regression. The relationship between the

screw and displacement was found to be linear, which is confirmed by the χ^2 value. Moreover, the refractive index of air was also calculated by finding the number of disappeared fringes for a change in pressure:

- At 293 K : $n_0 = 1.00038 \pm 0.00005$
- At 298 K : $n_0 = 1.00039 \pm 0.00001$
- At 303 K : $n_0 = 1.00039 \pm 0.00006$

Overall, the average of these values agreed with the accepted value of 1.000277 [source] within uncertainties, but each individual calculation did not. It is also important to recognize the potential for errors like instrumental uncertainties, manual counting, and variations in the environment during data collection(relative humidity). These results show that the Michelson interferometer is a powerful tool for a variety of precise measurements.

9 Appendix

Fringes Disappeared (±5)	Micrometer Reading (±0.005)	Actual Displacement (nm) (±1473)
0	21.27	309383
50	21.14	294650
100	21.04	279918
150	20.93	265185
200	20.83	250453
250	20.73	235720
300	20.66	220988
350	20.57	206255
400	20.49	191523
450	20.39	176790
500	20.28	162058
550	20.16	147325
600	20.08	132593
650	19.98	117860
700	19.91	103128
750	19.81	88395
800	19.72	73663
850	19.53	58930
900	19.45	44198
950	19.35	29465
1000	19.24	14733

Table 4: Full results for table 1

References

[1] *Interferometry*. University of Toronto, September 9, 2023.

[2] "Refractive Index Common Liquids, Solids and Gases." *Engineering ToolBox*, www.engineeringtoolbox.com/refractive-index-d_1264.html.

[3] *Michelson Interferometer with White Light - Department of Physics, Montana State University*, physics.montana.edu/demonstrations/video/6_optics/demos/michelsoninterferometerwithwh

[4] Harrison, D. M. (2001). *Error analysis in experimental physical science* . University of Toronto. https://faraday.physics.utoronto.ca/PVB/Harrison/ErrorAnalysis/All.pdf